Materials Letters 65 (2011) 1003–1006

Contents lists available at ScienceDirect

Materials Letters

journal homepage: www.elsevier.com/locate/matlet

Monodisperse porous pod-like hematite: Hydrothermal formation, optical absorbance, and magnetic properties

Wancheng Zhu [a,*], Xili Cui [a], Li Wang [a], Tao Liu [a], Qiang Zhang [b,*]

[a] Department of Chemical Engineering, Qufu Normal University, Shandong 273165, China
[b] Department of Chemical Engineering, Tsinghua University, Beijing 100084, China

ARTICLE INFO

Article history:
Received 26 November 2010
Accepted 27 December 2010
Available online xxxx

Keywords:
Hematite
Hydrothermal
Porous
Optical absorbance
Magnetic property

ABSTRACT

Uniform monodisperse porous silk-worm pod-like hematite (α-Fe_2O_3) superstructures were efficiently obtained via a facile hydrothermal route. This was realized via the co-precipitation of $FeCl_3$ and NaOH solutions at room temperature in the presence of H_3BO_3, followed by a mild hydrothermal treatment (150 °C, 12.0 h). The UV–vis band is mainly located in the far-UV region, with one intense broadband from 260 to 290 nm. The porous pod-like superstructures exhibit special magnetic properties with a remnant magnetization of 0.22 emu g^{-1} and a high coercivity of 3315.5 Oe at room temperature, indicating the as-obtained porous pod-like superstructures of a promising candidate for gas sensors, lithium ion battery, photocatalysis, and water treatment.

1. Introduction

The size and shape-dependent properties of nanomaterials have stimulated great efforts towards the controllable synthesis of nanostructures. To elucidate unique size/shape-dependent physico-chemical properties and explore their exciting applications, precise control of monodisperse architectural nanocrystals with uniform sizes is highly concerned [1]. Among various three-dimensional (3D) architectural metal and semiconductor nanocrystals, magnetic iron oxide systems illustrate their distinguished roles in nanomagnetism, photoanodes for efficient water splitting by sunlight, waste-water treatment, sensors, energy conversion and storage [1–5]. Hematite (α-Fe_2O_3) features non-toxicity, low cost, high stability, and environmental compatibility. Much effort has been made to prepare nanostructured hematite with various morphologies, such as monomorph hematite particles (e.g. peanuts [6], cubes [7], hexagonal platelets [8,9] and prism-shape [10]) and solid superstructures (e.g. microrings [11], columnar arrays [12], nanotube arrays [13], and urchin-like superstructures [14,15]). From the viewpoint of photocatalysis, sensor, and energy storage applications, monodisperse nanostructures with hollow cavities and uniform morphology are particularly desirable.

Very recently, novel hematite hollow architectures (e.g. hollow fibers [16] and microspheres [17–19]) and porous superstructures (e.g. branched nanostructure [3], mesoporous particles [20], nanocrystal clusters [21], and porous nanoflowers [22]) have emerged as the new highlights. Various synthesis routes, including forced hydrolysis (100 °C, 7–14 days) reaction [23], surfactant assisted solvothermal process [17,21], hydrothermal [24]/solvothermal [22] based or direct [21] calcinations (400–800 °C), were developed. However, some of them are time or energy consuming, and potential environmental malignant. It was still a challenge to directly acquire porous hematite superstructures by a facile, environmental benign, and low cost route [25]. In this contribution, novel monodisperse porous hematite superstructures with a silk-worm constructed pod-like morphology were synthesized by a facile hydrothermal route in the presence of boric acid. In addition, the optical absorbance and magnetic hysteresis loop of the porous hematite superstructures were also explored.

2. Experimental

2.1. Synthesis

In a typical procedure, 1.281 g of H_3BO_3 powder was poured into 10.1 mL of deionized (DI) water, then 9.3 mL of $FeCl_3$ (1.5 mol L^{-1}) solution was added, and finally 7.0 mL of NaOH (4 mol L^{-1}) solution was dropped into the above mixed solution under vigorous magnetic stirring at room temperature, with a molar ratio of $FeCl_3$:H_3BO_3:NaOH as 2:3:4. The resultant brown slurry was transferred into a Teflon lined stainless steel autoclave with a capacity of 44 mL. The autoclave was sealed and heated to 150 °C (heating rate: 2 °C min^{-1}) and kept in an isothermal state for 12.0 h, and then cooled down to room temperature naturally. The product was filtered, washed with DI water for three times, and finally dried at 80 °C for 24.0 h.

* Corresponding authors. Tel.: +86 537 4456301; fax: +86 537 4456305.
E-mail addresses: zhuwancheng@tsinghua.org.cn (W. Zhu), zhang-qiang@mails.tsinghua.edu.cn (Q. Zhang).

0167-577X/$ – see front matter © 2011 Elsevier B.V. All rights reserved.
doi:10.1016/j.matlet.2010.12.053

2.2. Characterization

Crystal phase and structure of the samples were identified by the X-ray powder diffractometer (XRD, D8-Advance, Bruker, Germany). Morphology and microstructure of the samples were examined by the field emission scanning electron microscopy (SEM, JSM 7401F, JEOL, Japan) and a high resolution transmission electron microscopy (TEM, JEM-2010, JEOL, Japan). Size distribution of the as-synthesized superstructures was estimated by direct measuring about 100 particles from the typical SEM images. The optical properties were examined by the UV–vis spectrophotometer (Cary 300, Varian, USA), with DI water as the dispersive medium. Magnetic measurements for the samples in the powder form were carried out at room temperature using a vibrating sample magnetometer (VSM 7307, LakeShore, USA) with a maximum magnetic field of 10 kOe.

3. Results and discussion

The XRD pattern, SEM images and size distribution of the hydrothermal products treated at 150 °C for 12.0 h in the absence or presence of H_3BO_3 were illustrated in Fig. 1. Each diffraction peak of both samples was easily indexed to that of the standard hematite (α-Fe_2O_3, PDF No. 33-0664, Fig. 1a). No impurity peaks were detected, indicating the as-synthesized products of pure hematite phase. Calculated from the Debye–Scherrer equation, the crystallite size along the [012] direction (i.e. D_{012}) and [104] direction (i.e. D_{104}) were of 31.7 and 27.3 nm, respectively. Without H_3BO_3 addition, the products became nonuniform (Fig. 1b). In contrast, the presence of H_3BO_3 promoted the formation of relatively uniform monodisperse porous superstructures with dominant silk-worm weaved pod-like and sparse pumpkin-like morphologies (Fig. 1c). A casually captured half α-Fe_2O_3 superstructure clearly showed that, the porous superstructure consisted of nanoparticles (NPs), which were located not only on the surfaces but also within the body (Fig. 1c_1). The statistical data (Fig.1d) demonstrated that *ca.* 84% of the pod-like α-Fe_2O_3 superstructures had a longitudinal length of 2.6–3.2 μm, revealing a narrow size distribution.

TEM images of the as-synthesized hematite superstructures are showed in Fig. 2. The superstructures were of relatively uniform pod-like morphology (Fig. 2a,b), containing multitudinal cavities with a diameter of 10–40 nm (Fig. 2a). This was in accordance with the SEM observation (Fig. 1c). The high magnification TEM image (Fig. 2c) corresponding to the blue dotted rectangular region of the selected individual superstructure (Fig. 2b) clearly illustrated that, the selected pod-like α-Fe_2O_3 was aggregated by multitudinal NPs. The diameter of the NPs in the superstructure was of 30–40 nm, quite similar to the crystallite size calculated from the Debye–Scherrer equation.

As reported, when sulfate or phosphate solution was used as additive, peanut-type hematite was obtained, which evolved from pseudocubic particles via an ellipsoidal shape [6]. In this letter, when H_3BO_3 was added, the porous pod-like hematite superstructures were acquired. To investigate its formation mechanism, the composition and morphology of the hydrothermal products obtained at 90–210 °C for 12.0–24.0 h were also monitored. When treated at 90 °C for 12.0 h or 105 °C for 1.0 h, the hydrothermal product was β-FeOOH, which first turned into compact pod-like hematite α-Fe_2O_3, and then into porous pod-like superstructure, with the increase in the temperature or prolongation of the time. Thus, formation of the porous pod-like α-Fe_2O_3 phase experienced a two-step phase transformation from Fe$(OH)_3$ to β-FeOOH and β-FeOOH to α-Fe_2O_3 [26].

The room temperature coprecipitation and hydrothermal conversion can be chemically expressed as follows:

$$FeCl_3 + 3NaOH \rightarrow Fe(OH)_3(gel) + 3NaCl \quad (1)$$

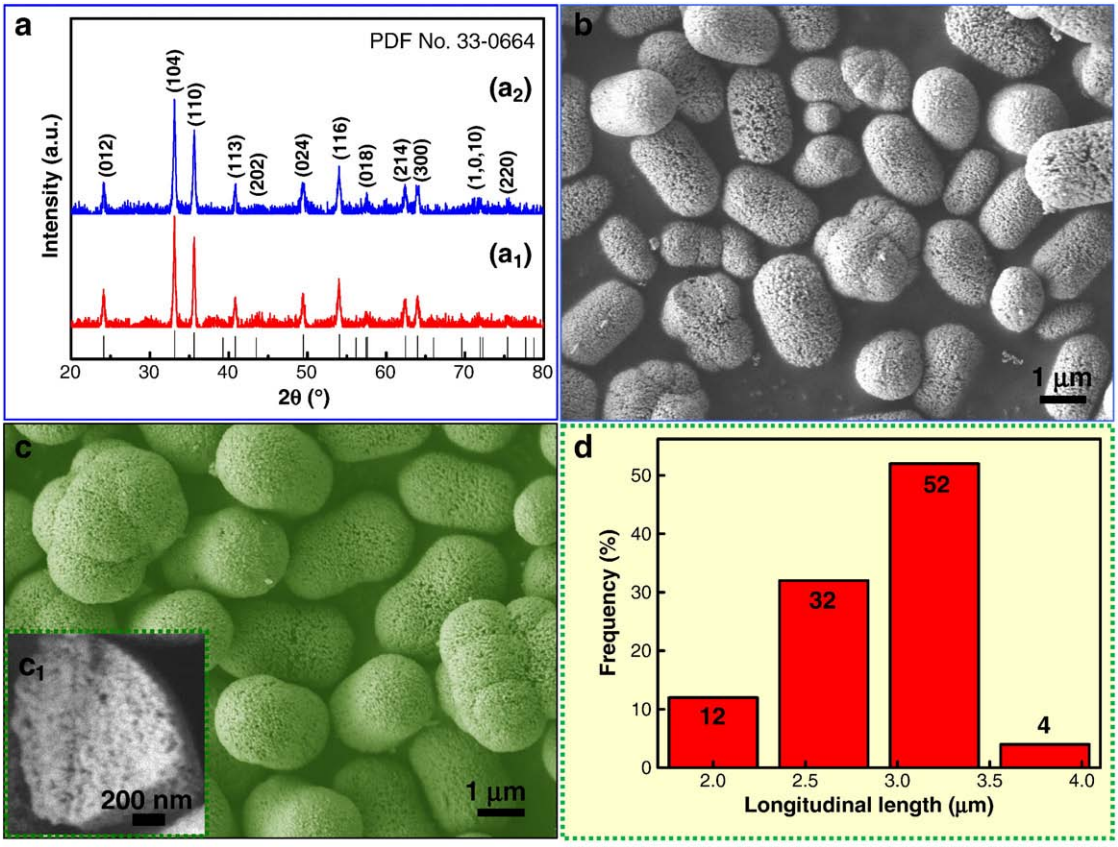

Fig. 1. XRD patterns (a), SEM images (b,c,c_1) and longitudinal length distribution (d) of the pod-like superstructures obtained in the absence (a_1,b) or presence (a_2,c,c_1,d) of H_3BO_3 at 150 °C for 12.0 h. Molar ratio: $FeCl_3$:H_3BO_3:NaOH = 2:0:4 (a_1,b), 2:3:4 (a_2,c). Vertical line (a): standard pattern of hematite (PDF No. 33-0664).

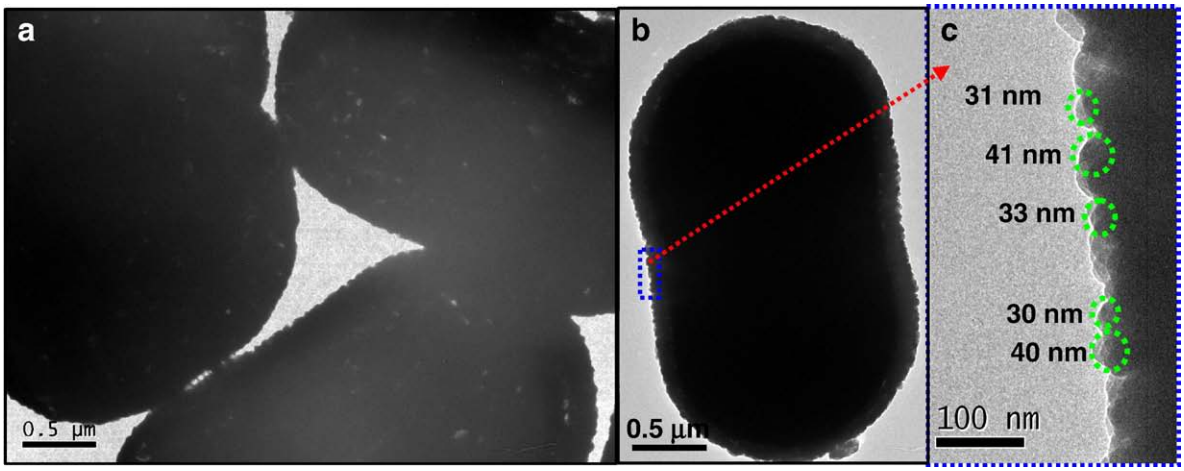

Fig. 2. TEM images of the hydrothermally synthesized pod-like superstructures obtained at 150 °C for 12.0 h. (For interpretation of the references to colour in this figure legend, the reader is referred to the web version of this article.)

$$Fe(OH)_3(gel) \rightarrow \beta\text{-}FeOOH + H_2O \quad (2)$$

$$2\beta\text{-}FeOOH \rightarrow \alpha\text{-}Fe_2O_3(mesoporous) + H_2O. \quad (3)$$

It is well illustrated that three types of electronic transitions occur in the optical absorption spectra of Fe^{3+} substances: (a) the Fe^{3+} ligand field transition or the d–d transitions, (b) the ligand to metal charge-transfer transitions, and (c) the pair excitations resulting from the simultaneous excitations of two neighboring Fe^{3+} cations that are magnetically coupled [27]. Fig. 3 shows the UV–vis spectrum of the porous pod-like α-Fe_2O_3. The UV–vis band is mainly located in the far-UV region, with one intense broadband from 260 to 290 nm, which was attributed to the electron transmission of Fe–O. In the visible region, just a weak absorption ranging from 550–600 nm was detected, which can be assigned to the $^6A_1 \rightarrow {}^4T_2(^4G)$ ligand field transitions of Fe^{3+} [27].

Fig. 4 shows the magnetic hysteresis loop of the porous pod-like hematite in the applied magnetic field sweeping from −10 to 10 kOe. Even at the maximum applied magnetic field, the hysteresis loop (M–H) does not reach saturation. The hysteresis loop of the porous pod-like hematite shows ferromagnetic behavior with a remanent magnetization of 0.22 emu g^{-1} and a coercivity of 3315.5 Oe at room temperature. The values of the remanent magnetization and coercivity of the pod-like hematite are higher than those of hollow hematite microspheres (remanent magnetization: 0.09 emu g^{-1}; coercivity: 1121.7 Oe) [19], urchinlike hematite (remanent magnetization: 4.68×10^{-3} emu g^{-1}; coercivity: 92.2 Oe) [15]. This was owing to the small primary NPs (*ca.* 30 nm) and structure of the pod-like hematite. Those particles can be easily separated from solution, indicating the superstructures of quite promising smart catalysts for efficient water splitting by sunlight and waste-water treatment.

4. Conclusions

Uniform monodisperse porous pod-like hematite (α-Fe_2O_3) superstructures have been synthesized via a facile hydrothermal route, which exhibited absorbance within ultraviolet and visible regions, as well as special magnetic properties with a remnant magnetization of 0.22 emu g^{-1} and a high coercivity of 3315.5 Oe at room temperature. The as-synthesized α-Fe_2O_3 superstructures can provide an alternative candidate for the potential applications in some emerging fields, such as gas sensors, photocatalysis, energy conversion/storage, water splitting and waste-water treatment, etc.

Acknowledgements

This work was supported by the State Key Laboratory of Chemical Engineering, China (No. SKL-ChE-09A02), the Project of Shandong Province Higher Educational Science and Technology Program, China (J10LB15), and the Excellent Middle-Aged and Young Scientist Award Foundation of Shandong Province, China (BS2010CL024).

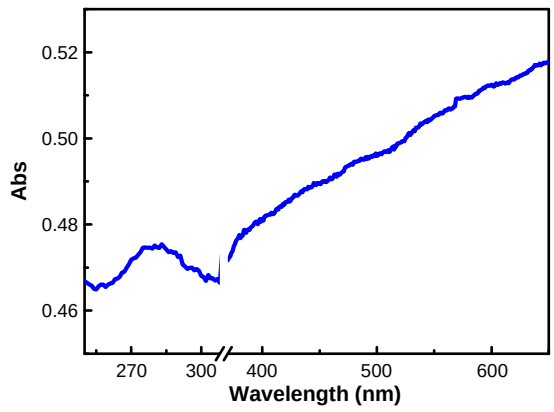

Fig. 3. UV–vis spectrum of the porous pod-like hematite dispersed in DI water.

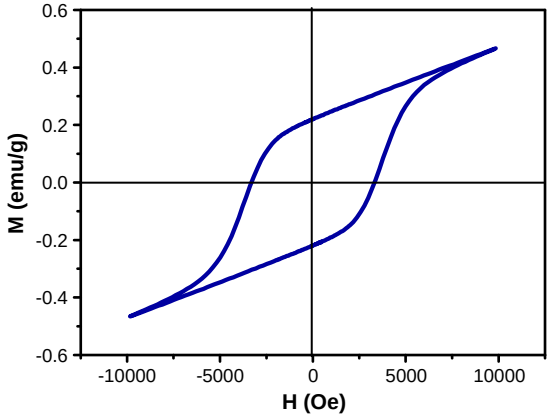

Fig. 4. Hysteresis loop of the as-synthesized porous pod-like hematite superstructures.

References

[1] Hu XL, Yu JC. Adv Funct Mater 2008;18:880–7.
[2] Saremi-Yarahmadi S, Tahir AA, Vaidhyanathan B, Wijayantha KGU. Mater Lett 2009;63:523–6.
[3] Yang HC, Mao XB, Guo YJ, Wang DW, Ge GL, Yang R, et al. CrystEngComm 2010;12:1842–9.
[4] Zhang ZH, Hossain MF, Takahashi T. Mater Lett 2010;64:435–8.
[5] Bharathi S, Nataraj D, Seetha M, Mangalaraj D, Ponpandian N, Masuda Y, et al. CrystEngComm 2010;12:373–82.
[6] Sugimoto T, Khan MM, Muramatsu A. Colloids Surf A 1993;70:167–9.
[7] Jia BP, Gao L. Cryst Growth Des 2008;8:1372–6.
[8] Peng DF, Beysen S, Li QA, Sun YF, Yang LY. Particuology 2010;8:386–9.
[9] Sun QJ, Lu XG, Liang GY. Mater Lett 2010;64:2006–8.
[10] Chaudhari NK, Kim HC, Son D, Yu JS. CrystEngComm 2009;11:2264–7.
[11] Zhong SL, Song JM, Zhang S, Yao HB, Xu AW, Yao WT, et al. J Phys Chem C 2008;112:19916–21.
[12] Li L, Koshizaki N. J Mater Chem 2010;20:2972–8.
[13] LaTempa TJ, Feng XJ, Paulose M, Grimes CA. J Phys Chem C 2009;113:16293–8.
[14] Zeng SY, Tang KB, Li TW, Liang ZH. J Phys Chem C 2010;114:274–83.
[15] Zhu LP, Xiao HM, Liu XM, Fu SY. J Mater Chem 2006;16:1794–7.
[16] Gong CR, Chen DR, Jiao XL, Wang QL. J Mater Chem 2002;12:1844–7.
[17] Li X, Yu X, He JH, Xu Z. J Phys Chem C 2009;113:2837–45.
[18] Wang JH, Ma YW, Wang DL, Gao ZS, Zhou YG, Song T. Mater Lett 2009;63:209–11.
[19] Song HJ, Li N, Shen XQ. Appl Phys A 2010, doi:10.1007/s00339-010-6072-7.
[20] Sivula K, Zboril R, Le Formal F, Robert R, Weidenkaff A, Tucek J, et al. J Am Chem Soc 2010;132:7436–44.
[21] Fang XL, Chen C, Jin MS, Kuang Q, Xie ZX, Xie SY, et al. J Mater Chem 2009;19:6154–60.
[22] Zeng SY, Tang KB, Li TW, Liang ZH, Wang D, Wang YK, et al. J Phys Chem C 2008;112:4836–43.
[23] Kandori K, Hori N, Ishikawa T. Colloids Surf A 2006;290:280–7.
[24] Zeng SY, Tang KB, Li TW, Liang ZH, Wang D, Wang YK, et al. J Phys Chem C 2007;111:10217–25.
[25] Gupta RK, Ghosh K, Dong L, Kahol PK. Mater Lett 2010;64:2132–4.
[26] Sugimoto T, Khan MM, Muramatsu A, Itoh H. Colloids Surf A 1993;79:233–47.
[27] Lian JB, Duan XC, Ma JM, Peng P, Kim TI, Zheng WJ. ACS Nano 2009;3:3749–61.